RESEARCH ARTICLE

Infrared signature of aero-engine exhaust plume's potential core and aircraft surface from direct bottom view

A. Bhatt[1,2] and S.P. Mahulikar[3,4]

[1]Aeronautical Development Agency, Bangalore, India
[2]Department of Aerospace Engineering, Indian Institute of Technology Bombay, Mumbai, Maharashtra, India
[3]IKERBASQUE, Basque Foundation for Science, Bilbao, Spain
[4]Departamento de Ingeniería Energética, Escuela de Ingeniería de Bilbao, University of the Basque Country UPV/EHU, San Mamés, Bilbao, Spain
Corresponding author: S.P. Mahulikar; Email: shripadprabhakar.mahulikar@ehu.eus

Abstract
Low-flying aircraft are susceptible to attacks by ground-launched infrared (IR)-guided man portable air defence system (MANPADS) and surface-to-air missiles (SAM). When seen from direct below, a dual band sensor can lock on to either exhaust plume or aircraft surfaces. Based on the magnitude of the IR signature, the missile can use any one source for the terminal guidance. In this study, the IR signature of the aircraft surface and potential plume core is analysed and compared from direct bottom view in different IR bands. In the Long Wave Infrared (LWIR) band, the surface emission is higher and in the Medium Wave Infrared (MWIR) band the plume emission is higher. The plume (MWIR) emission is higher than the surface (LWIR) emission for low Mach numbers, but as the Mach number increases the plume (MWIR) to surface (LWIR) emission ratio decreases, and at supersonic Mach numbers the surface LWIR signature is higher than the plume MWIR signature. The plume MWIR to surface LWIR ratio further depends on the engine power, altitude of operation and the emissivity of the aircraft surface. In the reheat mode, plume MWIR emission is always higher than the surface LWIR emission. The dual band IR detector can be a combination of short wave infrared (SWIR)-MWIR, SWIR-LWIR, and the MWIR-LWIR band. The MWIR-LWIR dual band combination is the best suited combination of IR windows for a dual band IR sensor/detector for aircraft application.

Nomenclature

I	radiation intensity (W/sr)
L	path-length (cm)
M	mach number (-)
P	pressure (Pa)
T	temperature (K)
e	infrared emission flux (W/m^2)
ε	emissivity (-)
k	absorption coefficient (cm^{-1})
m	mass flow rate (kg/s)
n	molar fraction (-)
τ	transmissivity (-)
λ	wavelength (μm)
i	intensity flux (W/m^2-sr)
r	recovery factor (-)

Subscripts

a	air
ac	aircraft
acs	aircraft surface
b	blackbody
bg	background
bot	bottom
cont	contrast
earth	earthshine
f	fuel
int	internal
p	plume
s	surface
sky	sky-shine
w	wall
∞	free stream
s9	static nozzle exit

Abbreviations

CD	convergent divergent
EM	electromagnetic
IR	infrared
LWIR	long wave IR (8–12 μm) band
LBL	line by line
LOWTRAN	low resolution atmospheric transmission
MANPADS	man portable air défense system
MOEA	multi-objective evolutionary algorithm
MSNBCK	multi-scale narrow band correlated-K
MWIR	medium wave IR (3–5 μm) band
SWIR	short wave IR (2–3 μm) band
SAM	surface to air missile

1.0 Introduction

With advancements in infrared sensing technologies, infrared (IR) missiles have become a serious threat to aviation. Advanced IR sensors based on the long wave irfrared (LWIR, 8–12 μm) band or the dual band of LWIR and medium wave infrared (MWIR, 3–5 μm) have IR imaging capabilities [1], which can distinguish an airborne vehicle from the background and identify the flying object as a friend or foe. The dual band sensor provides image fusion and all-weather capability to the missile. The IR signature is important for the detection, tracking and identification of an aircraft. The main sources of IR signature in an aircraft are surfaces heated due to aerodynamic heating, hot engine components and engine exhaust plume [2]. The aircraft external surfaces radiate primarily in the LWIR, followed by the MWIR and negligibly in the short wave infrared (SWIR, 2–3 μm) band. Hot engine components radiate in all three bands. Engine exhaust plume radiates mainly in the MWIR band followed by the SWIR band and negligibly in the LWIR band [3]. The IR signature received by the sensor is a function of the line of sight and the position of the sensor relative to the aircraft. The signal received by the sensor may vary depending on which parts of the aircraft are seen by the sensor. In addition, the IR signal is further attenuated by the presence of atmosphere between the aircraft and the sensor [4]. In the last few decades, IR guided missiles have been responsible for the majority of aircraft shootdowns. Man portable air defence system (MANPADS), e.g. 9K32 Strela-2, have been mainly responsible for this high rate of aircraft attrition [5]. MANPADS are SAMs that are typically fired from the shoulder, and have a range of 5–6km.

Due to the fact that these portable SAMs are mostly intended for low flying aircraft, it is important to study the IR signature of aircraft from the bottom side.

In the bottom view, the aircraft bottom surface and the exhaust plume are seen by the IR sensor. For majority of the fighter aircraft, the engine is concealed inside the rear fuselage, making it invisible from the bottom aspects. However, the variable exhaust nozzle, which is normally kept outside the rear fuselage, is visible to the IR sensor. The free stream Mach number changes the IR signature of the aircraft skin as well as the engine exhaust plume. Cha et al. [6] studied the effect of free stream Mach number on aircraft surface temperature for 4th and 5th generation aircraft. As the aircraft accelerates to a higher Mach number, the maximum skin temperature increases more rapidly than the average temperature. Lu et al. [7] showed that a decrease in skin temperature by 10K could lead to a decline of more than 8% of the IR intensity in front view. In the broadside of the aircraft, the drop in IR intensity is under 8%. Increase in Mach number results in increase in the engine power requirements; therefore, increasing the engine exhaust plume IR signature. Bhatt and Mahulikar [8] showed that potential plume core width and length increases with increase in free stream Mach number for an axisymmetric convergent divergent (CD) nozzle. Mahulikar et al. [9] studied infrared signatures of a low flying aircraft and optimised the rear fuselage emissivity. The aircraft was assumed to be flying at 1km above the SAM site. Emissions from aircraft rear fuselage due to heating by engine, exhaust plume, earthshine and attenuation due to atmosphere were modelled. Kim et al. [10] studied the susceptibility of a fighter aircraft. Temperature distributions, including aerodynamically heated surfaces and hot engine parts, were obtained by coupled computational fluid dynamics (CFD) simulations. The surface temperature of the aircraft was used to calculate the IR signature levels in the MWIR and LWIR bands depending on the detection aspect. Yanwan et al. [11] generated the IR images of automobiles and aircraft in LWIR band, a rendering method for generating infrared image was proposed. Atmospheric attenuation was considered for the image generation; however, engine exhaust plume was not considered for the simulations. Kajal and Mahulikar [12] analysed the IR signature of aircraft in LWIR band from frontal aspects. Aircraft nose cone IR signature due to aerodynamic heating was estimated and optimum emissivity to reduce IR signature of nose cone was proposed. Li et al. [13] proposed a real-time aircraft infrared imaging simulation platform that can perform a complete infrared imaging simulation of an aircraft. Four aspects were considered to calculate the real-time physical model of aircraft infrared radiation which was based on GPU and Cg programming languages. It involved a temperature model, an infrared radiation model of zero-distance, an atmospheric transfer model and an infrared imaging system effect model. The finite element method was introduced to solve the temperature field in real time. Huang and Ji [14] studied the impact of background radiation on LWIR characteristics of aircraft at high altitude. The reverse Monte Carlo ray tracing method was used to compute the infrared radiation signature of aircraft. The impact of atmospheric and ground radiation on the long-wave infrared radiation signature of aircraft at an altitude of 11km was analysed. The results showed that in the horizontal plane, the ratio of reflected background infrared radiation to self-infrared radiation is about 10% in summer and 7% in winter. Zhao and Zheng [15] used multi-objective evolutionary algorithm (MOEA) based on decomposition to solve the bi-objective optimisation problem of searching an appropriate group of nozzle's exit diameter and throat to exit diameter ratio. Objective of the optimisation was to select a diameter ratio which can reduce infrared signature radiation while reducing the loss of thrust. The optimisation results illustrate that dimension selection range and throat to exit diameter ratio have significant effects on the thrust loss and infrared signature level. Furthermore, the engine thrust was important in deciding nozzle exit diameter and throat diameter. Wang et al. [16] carried out a number of experiments to evaluate the infrared radiation characteristics of two-dimensional CD thrust vectoring nozzles with and without infrared suppression measures. Film cooling and low-emissivity coating, as two general infrared suppression measures, were adopted on the centrebody and divergent flaps of the nozzle. The wall temperature and infrared radiation characteristics were measured, and the infrared suppression effectiveness of film cooling and the low-emissivity coating were analysed. The investigation showed that the infrared radiation of the nozzle increases with the increase of the vectoring angle. The infrared radiation suppression of maximum 38% was achieved for 0° vectoring angle. Lin et al. [17] presented a scene-driven

coarse-to-fine aircraft target detection method. The method consisted of (1) pre-processing the image by combining the sharpened and enhanced images (2) the region of interest (ROI) was segmented by using the local mean variance of the image and a series of subsequent processing (3) target candidate areas were located by using the feature of local marginal distributions, and (4) aircraft was accurately detected by a novel aircraft shape filter. Cheng et al. [18] studied various configurations of serpentine nozzles to analyse the reduction in IR signature of the nozzle. The exhaust temperature of gases and nozzles was estimated using the CFD. The ray tracing method was used to estimate the IR signature level of different configurations. Haq and Huang [19] studied the IR signature of different elliptical exhaust nozzles. The aspect ratio (AR) at the exit of the nozzle was changed for different configurations. The study showed that the IR signature reduced from the side view by almost 80% in the MWIR band for the AR-10 nozzle. The combined IR signature from the exhaust plume and the nozzle exit plane in the MWIR spectral band reduced by 75% in the side view and 30% in the rear aspect. Yue et al. [20] developed a multi-scale narrow band correlated-k distribution (MSNBCK) model to simulate infrared radiation (IR) from an exhaust system of a typical aircraft engine. In the model, an approximate approach instead of a statistically uncorrelated assumption was used to treat overlapping bands in the gas mixture. The IR signature of the exhaust plume in the MWIR band was estimated using the MSNBCK model. The MSNBCK model significantly reduced the computing power compared to other models, and the results were comparable with the line by line (LBL) model. Mahulikar et al. [21] introduced the concept of infrared cross section and IR solid angle for analysing the IR signature of an aircraft. The lock-on range as a function of IRCS was formulated in the study. Similarly, various studies [22–28] have been carried out by the researchers on various aspects of engine exhaust plume IR signatures. Zhang et al. [29] provided integrated IR characteristics of aircraft skin and exhaust plume. The interaction between the aircraft and the plume IR were investigated by considering the reflection based on a bi-directional reflectance distribution function. Various influencing factors such as solar irradiation, ground reflection, aerodynamic heating and projection radiation from the background were also considered.

1.1 Motivation

IR-guided MANPADS are a serious threat to low-flying aircraft, these MANPADS can be based on single band or dual band sensor. A dual-band IR seeker can combine two bands from the SWIR, MWIR and the LWIR spectrums. If an IR detector operates in two IR windows, it can leverage the strengths of both bands and fuse the information to identify and ascertain the target with greater reliability. The SWIR band is capable of detecting hot engine components, exhaust nozzles, and exhaust plume. The peak emission in SWIR band is seen in temperature range 966–1,449K. Similarly, the MWIR band can also detect the engine's hot components, and exhaust plumes but offers additional capability to detect aircraft surfaces at high speeds. The peak emission in MWIR band is seen in the temperature range 579.6–966K. The LWIR band can identify the engine's hot components, exhaust nozzles and the entire aircraft external surfaces. However, engine exhaust plume is not visible in the LWIR band unless soot particles are present in the exhaust. Soot particle presence will make the plume to emit in all the three IR wave bands. The peak emission in LWIR band is seen in temperature range 241.5–362.25K. The main advantage of the LWIR band is that it can detect hot engine components and exhaust nozzles together with the aircraft surface emission at a temperature comparable to ambient air. The SWIR and MWIR bands cannot detect lower-temperature (ambient air temperature) surface emission. When detected from longer distance, the sensor having higher detection range is better, because the IR signal is from whole aircraft and not component wise. Identification of aircraft from a greater distance is challenging, and recognising different aircraft components becomes even more difficult. For the detections, it is not important if the signal is from the aircraft surface or the plume. However, towards the terminal guidance, the sensor, which can ascertain the target and differentiate between airframe and the plume is more useful. With the exact information of the target, the missile will cause greater damage to the airframe. If a missile directly hits the airframe, the ballistic damage due to direct hit will cause severe destruction to the aircraft. The direct hit can cause complete loss of aircraft or it can make aircraft uncontrollable.

However, if the missile detonates near the plume, the aircraft will suffer damage from blast fragmentation, which will be less severe than a direct hit. Thus, it is important to target aircraft surfaces towards the terminal guidance.

1.2 Objectives and scope

The objective of this study is to analyse the IR signature of an aircraft when seen from the bottom, and compare the IR signature of the aircraft skin and engine exhaust potential core in SWIR, MWIR and LWIR bands. Study the effect of free stream Mach number on the ratio of plume to aircraft surface IR signature. Additionally, it aims to compare the IR signatures of the exhaust plume and aircraft surface in two different IR bands. The comparison will help dual-band IR detectors in selecting the most effective IR bands for targeting an aircraft. The role of MWIR or LWIR band towards the terminal guidance is also discussed.

2.0 IR signature of aircraft bottom surfaces

The IR signature (IR contrast) of the aircraft in a wavelength band $(\lambda_1 - \lambda_2)$ is given by $I_{cont} = I_{ac} - I_{bg}$. Where I_{ac} is the IR intensity of the aircraft which includes the internal emission, and the reflected radiation. I_{bg} is the radiation of the background replaced by the aircraft. When the aircraft is seen from the bottom, the background will be sky. The IR radiation flux from the bottom surface of the aircraft will be:

$$i_{s-cont} = i_{s-bot} - i_{sky} \left(\text{W/m}^2 - \text{sr} \right) \tag{1}$$

The i_{s-bot} consists of IR (internal) due to the surface temperature of the bottom surfaces and the reflected skyshine, sunshine and earthshine. Normally the sky reflection from the aircraft is very low and can be neglected. The earthshine (earth radiation reflection from the aircraft) is mostly important from the bottom view of the aircraft and is significant for the low-flying aircraft [30]. The sunshine (reflection of sun radiation from the a/c) is significant in the SWIR band followed by the MWIR band and negligible in LWIR band. In the present study, it assumed that aircraft is flying in the night sky, thus sunshine emission is neglected. The IR intensity flux, which is defined as radiation energy emitted in a given direction, per unit normal area, and per unit solid angle leaving the aircraft's bottom surface can be given by:

$$i_{s-bot} = i_{s-bot-int} + i_{s-bot-earth} \tag{2}$$

The $i_{s-bot-int}$ is the intensity flux due to the surface temperature of aircraft bottom surfaces, given by $i_{s-bot-int} = \varepsilon_{acs} e_{s-bot-int}/\pi$, where ε_{acs} is the emissivity of the aircraft bottom surface and $e_{s-bot-int}$ is the blackbody emission of the aircraft bottom surface in the wavelength band $\lambda_1 - \lambda_2$. The black body emission $(e_{s-bot-int})$ at T_w wall surface temperature is given by:

$$e_{s-bot-int(\lambda 1 - \lambda 2)} (T_w) = \int_{\lambda_1}^{\lambda 2} \frac{C_1}{\lambda^5 \left(\exp\left(\frac{C_2}{\lambda T}\right) - 1 \right)} \tag{3}$$

Where $C_1 = 0.596 \times 10^{-16}$ W-m^2 and $C_2 = 0.014387$ m-K. The aircraft bottom surface temperature depends on the flight altitude and Mach number. The maximum temperature that the bottom surface can attain for subsonic to supersonic Mach number range is the recovery temperature (T_r). In the present study the bottom surface temperature is assumed to be equal to the recovery temperature T_r, given by:

$$T_r = T_\infty \left(1 + r \frac{\gamma - 1}{2} M_\infty^2 \right) \tag{4}$$

Where T_∞ is the free stream static temperature at the given altitude, M_∞ is the free stream Mach number, γ is the specific heat ratio, and 'r' is the recovery factor. The recovery factor is given by $= Pr^n$, $n = 0.5$ for laminar flow and 1/3 for turbulent flow. The assumption of $T_w = T_r$ holds good for

subsonic and supersonic flows; it is conservative for the current study. The earthshine reflection from the bottom surface of the aircraft is estimated as $i_{s\text{-}bot\text{-}earth} = (1-\varepsilon_{acs})\,G_{earth}$, where G_{earth} is the earth irradiance on the aircraft's bottom surface. It is estimated using the methodology of Mahulikar et al. [30,31]. In the current study the earth's surface temperature is assumed to be 30°C and the earth's emissivity (ε_{ed}) is taken as 0.95. The transmission from the earth to the aircraft bottom surface is calculated using LOWTRAN 7 [32]. The sky emission i_{sky} is given by $\varepsilon_{sky}e_{sky}/\pi$, where ε_{sky} is the emissivity and e_{sky} is the blackbody radiation of the sky at the ambient air temperature, for the given altitude. Berger et al. [33] have used LOWTRAN and sounding balloon data to provide a relationship of total sky emissivity as a function of altitude. The sky emissivity in the SWIR band and MWIR is approximately 1.0, since the temperature of sky is low, the overall sky emission in the SWIR and MWIR band is insignificant. In the LWIR band, the sky emission is significant but the sky emissivity is well below 1.0, and varies with altitude. At sea level, the sky emissivity in the LWIR band is 0.47 and decreases as the altitude increases, at 4km altitude it is equal to 0.10. The IR signature (contrast) of aircraft is $i_{s\text{-}bot} - i_{sky}$, the sky emission reduces the overall IR magnitude. At lower altitudes (1–2km), the sky temperature and sky emissivity (LWIR) are higher compared to the higher altitudes, therefore, sky emission has significant contribution to overall IR signature of the aircraft. At higher altitudes, since the ambient temperature as well the sky emissivity is low, the contribution of sky emission in IR signature (LWIR) is insignificant. For example, at sea level $M_\infty = 1$, the IR signature due to aircraft surface is 216.36W/m^2-sr, the sky emission is 46.44W/m^2-sr, and the IR contrast is 169.92W/m^2-sr. While, at $h = 4$km, $M_\infty = 1$, the IR signature due to aircraft surface is 140.63W/m^2-sr, the sky emission is 5.979W/m^2-sr, and IR contrast is 134.65W/m^2-sr. The IR signature is reduced by 21.4% at sea level, and at $h = 4$km, it is reduced by 4.125% by the sky emission. The sky emission contribution continues to reduce with increase in altitude.

Using the data from Fig. 4 of Berger et al. [33] the spectral data is extracted and linearly extrapolated to the 6km ISA condition. At this altitude, the ε_{sky} in the LWIR band is 0.04. Figure 1 shows the variation of radiation contrast flux intensity of the aircraft bottom surface with M_∞ for the three IR bands. The IR contrast of the aircraft bottom surface increases with M_∞ due to increase in the aircraft surface temperature from aerodynamic heating. When the aircraft emissivity is equal to one, the total IR signature of the aircraft is due to the surface temperature of aircraft alone. When ε_{acs} is 0.5, some part of the aircraft bottom surface radiation is contributed by the earthshine also, and when ε_{acs} is 0, the aircraft bottom surface radiation is due to the earthshine alone. The earthshine does not depend on the M_∞, thus when ε_{acs} is 0, the total IR radiation from aircraft bottom surface will not change with M_∞. From Fig. 1, it is also seen that the IR signature of the aircraft bottom surface is dominant in the LWIR band followed by the MWIR band and negligible in the SWIR band. It is because the aircraft surface temperatures due to aerodynamic heating in the considered range of M_∞ are below 400K. Based on Wien's displacement law, the IR radiation peaks in the LWIR band at these temperatures. At supersonic Mach numbers, some radiation is seen in the MWIR band, but for the range of Mach numbers under study, the MWIR emission is still lower than the LWIR emission. The temperatures at these Mach numbers are not high enough to radiate in the SWIR band. In the SWIR band the peak radiation occurs in temperature range 966–1,499K.

3.0 IR signature of exhaust plume potential core from bottom view

The plume of an aero-engine has a unique structure that resembles an onion peel with various iso-concentrate/isotherm layers. The innermost part of the plume is known as the potential core, which is relatively shorter than the overall length of the plume. The potential core is the region within the plume where there is no mixing of exhaust constituent with the atmosphere. The temperature and molar concentration of CO_2 and H_2O (vap.) are constant and highest in the potential core plume region. The plume potential core is the maximum contributor to the IR signature of the exhaust plume. In this study, the IR signature of the plume potential core is studied and compared with the aircraft surface radiation.
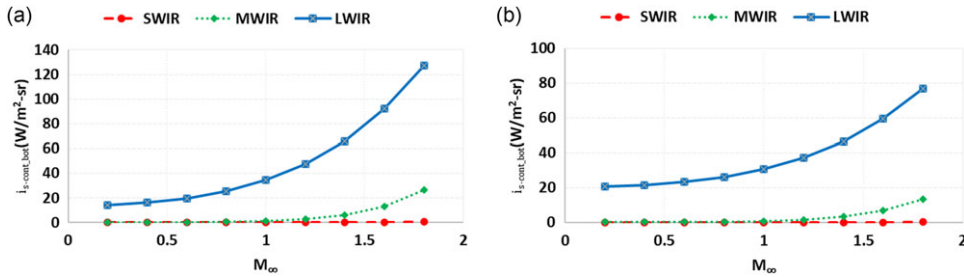
Figure 1. *IR contrast intensity of aircraft surface vs. M_∞ at 6km, ISA, (a) $\varepsilon_{acs}=1$, (b) $\varepsilon_{acs}= 0.5$.*

Unlike opaque solid surfaces, plume is a transparent gaseous medium, therefore, the background radiation will also pass through it. The IR contrast intensity of the plume from the bottom view, in a given IR band, can be estimated as $i_{p-cont} = i_{p-bot} + \tau_{plume} i_{sky} - i_{sky}$. The IR intensity due to the plume is given by $i_{p-bot} = i_{p-bot-int} + i_{p-bot-earth}$, where $i_{p-bot-int}$ is the IR intensity due to the plume gases and $i_{p-bot-earth}$ is the reflected earthshine from the plume. Since the molecular dimension of the gaseous molecule is small compared to the wavelength of IR-EM spectrum, scattering, and therefore, the reflectivity of the plume can be assumed to be zero, making $i_{p-bot-earth}$ zero. Thus, making $i_{p-bot} = i_{p-bot-int}$. However, if soot particles are present in the plume, scattering cannot be neglected. The soot particles emit radiation in all IR wavelengths; thus, changing the IR signature behaviour of the plume. Presence of soot particles has not been considered in this study. The IR intensity from the plume gases can be calculated as:

$$i_{p-bot-int} = \varepsilon_p e_{b_p}/\pi \qquad (5)$$

Where e_{b_p} is black body emissive power of the plume in given wavelength band. Unlike aircraft surface, engine exhaust plume emissivity (ε_p) has spectral dependence, ε_p is different in different IR bands. If the hydrocarbon fuel used for combustion is assumed pure and the combustion is complete, then the engine exhaust plume consists of CO_2, H_2O (vap.), O_2, and N_2. The constituents such as CO, NO_x and SO_x can also be present in the plume but their contribution to overall IR signature of plume is negligible [34]. O_2 and N_2 are inert to the IR radiation, while CO_2 and H_2O participates in IR radiation. The emission in different IR bands by the CO_2 and H_2O is dependent on their molar concentration, plume exhaust temperature and the exhaust pressure. In the present study, Gasturb14 [35] is used for obtaining data for a turbojet engine. The design point for the engine is assumed sea level static and the data is generated for the off-design conditions, i.e. 6km, ISA for various M_∞. The design point for a fighter aircraft can be different than the sea level static; however, the design point does not affect the trend of engine temperature with Mach number. This may change the magnitude of IR signature at off design points but overall trends will remain the same. Majority of the military turbofan engines use afterburners; wherein additional fuel is burned in the jet pipe of the afterburner to increase the thrust for a shorter duration. Max dry mode (maximum dry mode) is the maximum power of the engine without an afterburner; maximum reheat mode (max reheat mode) is the maximum power of the engine with a full afterburner engaged. In the present study, the IR signature of the exhaust plume is analysed in max dry mode and max reheat mode of the engine. Table 1 shows the engine data generated using Gasturb14. The fuel is considered to be Jet A1, the chemical formula for which is approximately $C_{11}H_{21}$ [36]. The mole fractions of the exhaust plume constituents are estimated by assuming complete combustion [37]. Table 2 shows the molar fraction of CO_2 and H_2O (vap.) for different M_∞ at 6km, ISA conditions for maximum dry power of engine.

The emissivity of engine exhaust gases can be calculated using the LBL model, band model, or the global models. The LBL model is the most accurate method [38] for estimating the radiation properties of gaseous medium using spectral databases such as HITEMP and HITRAN. In the present study the LBL model is used for estimation of the radiation properties of CO_2 and H_2O using HITRAN 2016 [39]

Table 1. *Gasturb data for 6km, ISA*

M_∞	Maximum dry mode				Maximum reheat mode			
	m_f (kg/s)	m_a (kg/s)	P_{s9} (kPa)	T_{s9} (K)	m_f (Kg/s)	m_a (kg/s)	P_{s9} (kPa)	T_{s9} (K)
0.2	1.1204	53.585	55.574	727.67	3.0749	53.585	56.141	1,467.5
0.4	1.1835	56.916	59.052	728.45	3.2548	56.916	59.654	1,469.3
0.6	1.2916	62.733	65.118	729.45	3.5657	62.733	65.777	1,471.6
0.8	1.4551	71.547	74.363	731.63	4.0385	71.547	75.105	1,476.2
1	1.6769	83.625	87.124	735.39	4.6887	83.625	87.98	1,483.8
1.2	1.9372	97.905	102.47	742.02	5.4686	97.905	103.45	1,496.6
1.4	2.1805	112.34	118.06	748.29	6.242	112.34	119.16	1,508.6
1.6	2.3582	124.47	131.34	754.77	6.877	124.47	132.53	1,520.9
1.8	2.4859	136.09	143.8	757.97	7.4266	136.09	145.08	1,526.9

Table 2. *Molar fraction and transmissivity of engine exhaust constituents, 6km, ISA, max dry*

M_∞	n_{CO2}	n_{H2O}	n_{O2}	n_{N2}	τ_{CO2} (SWIR)	τ_{H2O} (SWIR)	τ_{CO2} (MWIR)	τ_{H2O} (MWIR)	τ_{CO2} (LWIR)	τ_{H2O} (LWIR)
0.2	0.06439	0.0614	0.1077	0.7664	0.999	0.998	0.982	0.999	0.999	0.999
0.4	0.06399	0.0610	0.1083	0.7666	0.999	0.998	0.981	0.999	0.999	0.999
0.6	0.06338	0.0605	0.1092	0.7668	0.999	0.998	0.979	0.999	0.999	0.999
0.8	0.06263	0.0597	0.1104	0.7671	0.999	0.998	0.977	0.999	0.999	0.999
1	0.06178	0.0589	0.1117	0.7674	0.999	0.998	0.974	0.999	0.999	0.998
1.2	0.06098	0.0582	0.1130	0.7677	0.999	0.997	0.970	0.999	0.999	0.998
1.4	0.05985	0.0571	0.1148	0.7681	0.998	0.997	0.967	0.999	0.999	0.998
1.6	0.05846	0.0558	0.1170	0.7686	0.998	0.997	0.964	0.999	0.999	0.998
1.8	0.05642	0.0538	0.1202	0.7694	0.998	0.997	0.962	0.999	0.999	0.998

database. The transmissivity of individual gas molecule is given by: $\tau_i = \exp(-k_i.N_i.L)$, where τ_i is the transmissivity by the individual gas, k_i is the absorption coefficient of the gas molecule at given pressure and temperature, N_i is the molecular number density given by: $N = (2.6867 \times 10^{19}) . \left(\frac{273.15}{T}\right) . P_{mol}$, and L is the pathlength in cm. The absorption coefficient (k_i) is estimated using the molar fraction, exhaust pressure and temperature of the engine exhaust constituents (CO_2 and H_2O) at the nozzle exit. The transmission calculation depends on the line of sight (LOS) or the pathlength (L) through the potential plume core. The shape of potential core for axisymmetric nozzles is approximately like a cone with the base diameter of the engine exhaust. From the bottom view, the pathlength can be conservatively taken equal to exhaust diameter of the nozzle.

The transmissivity of the potential plume core is high in all the IR band for the max dry mode. Plume is almost transparent in LWIR band for both CO_2 and H_2O (Table 2). In the MWIR band transmissivity of the CO_2 decreases with the M_∞, and ranges from 0.98 to 0.96. The H_2O (vap.) does not radiate in MWIR band, it's transmissivity in the MWIR band ranges 0.997–0.998. Therefore, the total emission in MWIR band is due to CO_2 alone. In the SWIR band, for $M_\infty < 1.2$, the transmission due to CO_2 is of the order of 0.999; at supersonic speeds (>1.2) the transmissivity is of the order of 0.998. The H_2O transmission in SWIR band is of the order of 0.997. Overall, in the SWIR band, the transmissivity of exhaust plume is very high. For the homogenous gas mixtures, the overall mean transmissivity ($\overline{\tau}$) in the given IR band is the product of transmissivity of individual gas constituent, given by: $\overline{\tau} = \prod_{i=1}^{n} \overline{\tau_i}$. Figure 2 shows the variation of plume transmissivity in MWIR with M_∞. The transmissivity decreases with M_∞.

Table 3. *Emissivity of plume potential core, 6km, ISA, max dry and max reheat*

M_∞	T_{s9} (K) dry	T_{s9} (K) reheat	ε_dry (SWIR)	ε_dry (MWIR)	ε_dry (LWIR)	ε_reheat (SWIR)	ε_reheat (MWIR)	ε_reheat (LWIR)
0.2	727.7	1,467.5	0.00149	0.01559	0.00012	0.00180	0.01801	0.00079
0.4	728.5	1,469.3	0.00157	0.01637	0.00013	0.00191	0.01896	0.00085
0.6	729.5	1,471.6	0.00171	0.01770	0.00014	0.00209	0.02059	0.00094
0.8	731.6	1,476.2	0.00193	0.01965	0.00016	0.00236	0.02301	0.00109
1.0	735.4	1,483.8	0.00223	0.02220	0.00019	0.00273	0.02618	0.00128
1.2	742.0	1,496.6	0.00257	0.02502	0.00023	0.00316	0.02974	0.00151
1.4	748.3	1,508.6	0.00289	0.02755	0.00027	0.00358	0.03310	0.00173
1.6	754.8	1,520.9	0.00311	0.02932	0.00030	0.00392	0.03568	0.00192
1.8	758.0	1,526.9	0.00327	0.03057	0.00032	0.00422	0.03793	0.00208
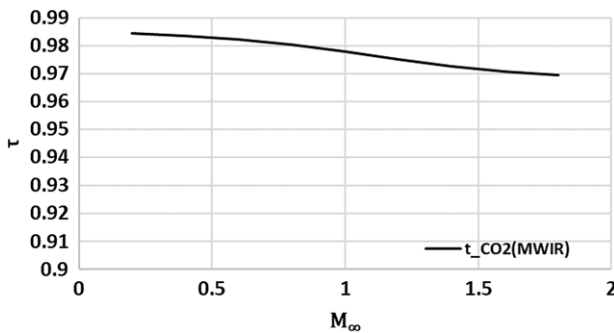
Figure 2. *Variation of CO_2 transmissivity in MWIR band with M_∞, 6km ISA, max dry.*

The emissivity of the plume is calculated by assuming reflection as zero, therefore, mean emissivity ($\bar{\varepsilon}$) in the given IR band is equal to $1 - \bar{\tau}$. The mean emissivity of the potential plume core in different IR bands for 6km altitude is given in Table 3. The emissivity of the plume is maximum in the MWIR band, followed by the SWIR band, and minimum in the LWIR band. With an increase in M_∞, the thrust requirement of the engine increases, leading to increased pressure and temperature of the plume. The IR signature of the plume is dependent on temperature and emissivity. The plume emissivity is dependent on, temperature, pressure and molar fraction of the IR participating gases (CO_2 and H_2O). With an increase in pressure and the temperature of the exhaust gases, the emissivity of CO_2 and H_2O increases due to collision broadening. Collision broadening is the broadening of spectral lines due to increased collisions between the molecules of IR participating gas (e.g. CO_2 and H_2O). Increased pressure leads to higher density of molecules in the plume, resulting in an increase in the frequency of collisions between molecules. Higher temperature increases the mean kinetic energies of the gaseous molecules leading to high frequency of collision. Thus, increase in pressure and temperature leads to increase in plume emissivity due to collision broadening. Although the fuel flow rate increases with an increase in M_∞, the molar fraction of CO_2 and H_2O decreases slightly (in the maximum dry mode of the engine), it is because, the increase in fuel flow rate is lesser compared to the increase in the air mass flow rate to the engine (Tables 1 and 3). For example, from Mach number 0.2 to 0.4, the increase in fuel flow is by 5.63%, but the increase in air flow rate is by 6.21%. The decrease in molar fraction has the effect of decreasing emissivity. As the Mach number (M_∞) increases, the emissivity of the plume rises due to the collision broadening of CO_2 and H_2O molecules. In the maximum afterburner mode, nearly all available oxygen is consumed to burn the additional fuel, leading to a higher molar fraction of CO_2 and H_2O. However, in the afterburning mode, the molar fraction of CO_2 and H_2O shows negligible change with increase in the Mach number. When the engine shifts from maximum dry mode to maximum reheat
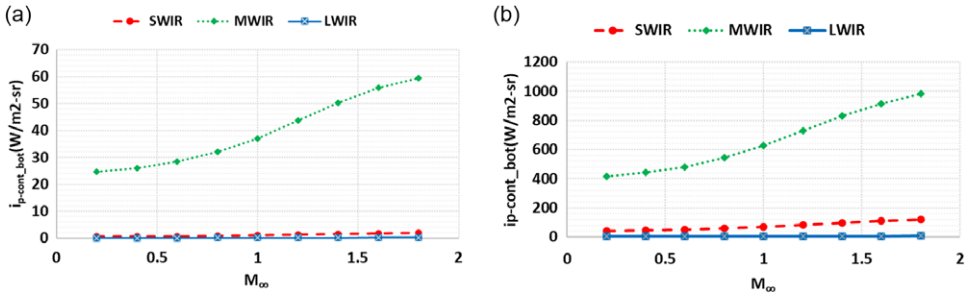
Figure 3. *Variation IR intensity of the plume with M_∞, 6km, ISA, (a) Max Dry, b) max reheat.*

mode at a given M_∞, emission and absorption increase because of the rise in temperature, pressure, and the concentration of CO_2 and H_2O.

The IR contrast of the plume is be given by $i_{p\text{-}cont} = i_{p\text{-}bot} + \tau_{plume}i_{sky} - i_{sky}$. As seen from Tables 2 and 3, plume is transparent in the LWIR band, transmission in the SWIR band is close to 0.99 In the MWIR band, it ranges from 0.96 to 0.98. Since the sky emission is negligible in the SWIR and MWIR band, $\tau_{plume}i_{sky} - i_{sky}$ is approximately equal to zero in all three IR bands. Thus, the IR contrast of the plume can be given by $i_{p\text{-}cont} = i_{p\text{-}bot}$. The IR contrast of the plume is approximately equal to the self-emission from the plume in all three IR bands. Figure 3(a) shows the variation of IR intensity of the plume from the bottom view in three IR bands for maximum dry mode of the engine. The IR intensity of the plume is maximum in the MWIR band followed by the SWIR band and negligible in the LWIR band. In the MWIR band CO_2 is the only emitter, in the SWIR band both CO_2 and H_2O emits the radiation, but the overall emission in MWIR is 30–37 times more than in SWIR band. The IR intensity increases with M_∞ because of two effects (1) rise in the exhaust gas temperature, and (2) increases in the plume emissivity both in SWIR and MWIR band. The emission of both CO_2 and H_2O is negligible in LWIR band.

In the reheat mode of the engine, the fuel flow rate, and the exhaust gas temperature increase significantly compared to the max dry mode. Figure 3(b) shows the variation of plume IR emission for max reheat mode of the engine, when seen from below for 6km ISA conditions. The plume emission in max reheat mode is significantly high compared to the max dry mode. For the MWIR band the rise is almost 16 times, 66 times for the SWIR band and 25 times for the LWIR band. The high emission is mainly due to the high exhaust gas temperature, which is almost doubled. For $M_\infty = 1.8$, the temperature rise is approx. 2.09 times, and the emissivity has increased by 21 % in MWIR band. The increase in IR signature is more pronounced in the SWIR band compared to the MWIR. At $M_\infty = 1.8$, the ratio of MWIR to SWIR radiation is 8.16 in max reheat mode, compared to 30 in the max dry mode. This difference is due to the rise in exhaust gas temperatures, which increase from 1,467K in max dry mode to 1,526K in the max reheat mode. The peak radiation for these temperatures occurs at wavelengths of 1.97 and 1.89μm, respectively, which is near to the SWIR band. Although the radiation in max reheat mode peaks in the SWIR band, the overall IR radiation of the plume is lower in SWIR compared to the MWIR band. This is because: (1) The emissivity of the plume is lower in the SWIR band and (2) the SWIR band has a narrower bandwidth compared to the MWIR band. Table 3 shows the comparison of exhaust gas temperature and emissivity for max dry and max reheat mode of the engine.

Figure 4 shows the variation of IR intensity of plume's potential core with altitude from direct bottom view at $M_\infty = 1$. The IR intensity is negligible across all altitudes in the LWIR band. In the SWIR band, the plume's IR intensity is very low, and it decreases further with the altitude. Similarly, in the MWIR band, the IR intensity decreases continuously with increase in the altitude. This is because, as the aircraft gains the altitude at a constant M_∞, the thrust requirement of engine reduces, leading to reduction in exit pressure and temperature. The lower temperature causes a direct decrease in the radiation intensity. Additionally, the reduction in pressure, temperature and the molar fraction of CO_2, H_2O leads to decrease
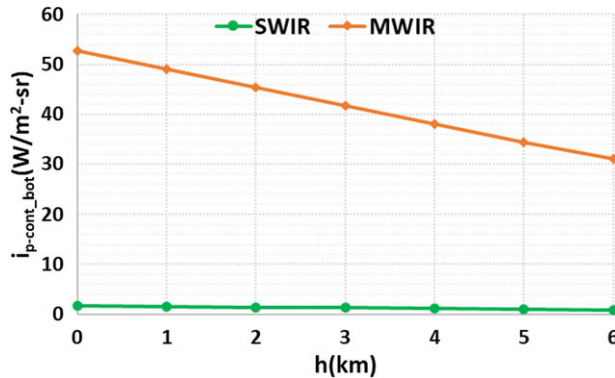
Figure 4. *Variation of plume IR intensity flux with altitude, $M_\infty = 1$, ISA, max dry.*

in the emissivity of the exhaust plume in all the three IR bands. Consequently, the overall IR intensity of the plume's potential core decreases with increasing altitude at a constant M_∞.

4.0 Comparison of aircraft surface and plume potential core radiation from bottom view

The radiation characteristics of the aircraft surface and exhaust plume differ significantly. The aircraft surface radiates in all the IR wavelengths; while the plume is a select band emitter, radiating predominantly in specific IR bands. The aircraft external surface temperature, caused by the aerodynamic heating, is comparatively lower than the engine exhaust temperature. The peak radiation from the aircraft external surface occurs in the LWIR band, while the peak radiation of the engine plume occurs in the MWIR band for max dry mode and in the SWIR band for max reheat mode. For example, the maximum adiabatic wall temperature (recovery temperature) of the aircraft bottom surface for $M_\infty = 1.8$ at 6km altitude is 395K, while the exhaust gas temperature in the max dry mode is of the order of 795K. Thus, the peak radiation wavelength of the aircraft surface is 7.33μm, while the plume peak radiation occurs at 3.64μm. In the max reheat mode, the plume emission peaks near the SWIR band. For example, at $M_\infty = 1.8$ at 6km altitude, the exhaust gas temperature is approximately 1,526K, which corresponds to peak emission wavelength of 1.89μm.

From Figs 1 and 3, it is evident that the aircraft surface radiation is important in the LWIR band, while the plume radiation is prominent in the MWIR band. However, when the aircraft is flying at supersonic speed, the aircraft surface temperature is high enough to emit in the MWIR band. Figure 5 presents the variation of plume to surface radiation ratio with M_∞ in three IR bands. The plume /surface IR is referred as 'radiation ratio' henceforth in this document. The emissivity of the aircraft bottom surface (ε_{acs}) is considered to be 1 for the comparison. When ε_{acs} is 1.0, the surface radiation is maximum for a given temperature. A decrease in emissivity reduces the radiation intensity, affecting the magnitude and the radiation ratio, but the overall trend remains unchanged. The radiation ratio in MWIR band decreases with M_∞ (Fig. 5a), because, the aircraft surface temperature increases with increase in M_∞. At high M_∞, surface temperatures are high enough to emit in the MWIR band. The MWIR radiation ratio trend with M_∞ is similar for both maximum dry and reheat mode of the engine. At low Mach numbers, the plume signature is significantly higher than the surface IR signature. At $M_\infty = 0.3$, the MWIR radiation ratio is of the order of 289 for max dry mode and 4,891 for max reheat mode. At $M_\infty = 1.8$, the MWIR radiation ratio is 2.2 for max dry mode and 45.9 for max reheat mode. Normally fighter aircraft do not fly at speeds higher than $M_\infty = 2$, therefore, for a fighter aircraft, potential plume core IR signature is always higher than the surface IR signature in the MWIR band.

Figure 5(b) illustrates how the radiation ratio varies with M_∞ in the LWIR band. Although the plume temperature is higher compared to the aircraft bottom surface, the emissivity of the plume potential

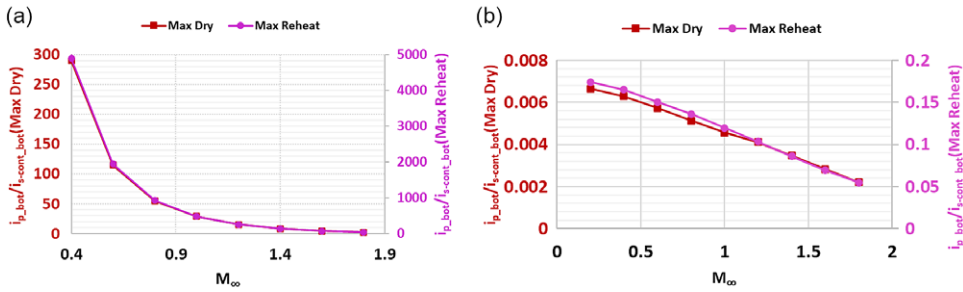**Figure 5.** *Comparison of plume and aircraft surface emission from direct bottom view, 6km ISA,* $\varepsilon_{acs} = 1$, *(a) MWIR, (b) LWIR.*

core is negligible in LWIR band. The plume potential core is almost transparent in the LWIR band, and the emission is negligible in both max dry and max reheat mode. The LWIR radiation ratio is of the order of 10^{-3} for the max dry mode and 10^{-1} for the max reheat mode. Since the SWIR signature of the aircraft surface and the potential plume core is negligible for the max dry mode, it is not plotted in Fig. 5. However, in the max reheat mode, the SWIR signature of the plume's potential plume core becomes significant.

The above comparison of the plume and aircraft bottom surface is carried out for a single band IR sensor. Nowadays, IR sensors have the capability to detect the IR radiation in two different IR bands. Dual band sensor can be a combination of SWIR, MWIR and LWIR band. The dual-band capability offers better target identification and reduces false alarms compared to a single band sensor. The plume is a major emitter in the MWIR band followed by SWIR band, and negligible in LWIR. If soot particles are present in the plume, they emit in all the IR bands. Conversely the aircraft bottom surface is a major emitter in the LWIR band followed by MWIR band, and negligible in SWIR. When a dual-band (MWIR-LWIR) or (SWIR-LWIR) seeker observes an aircraft from a direct bottom view, it always has an option to lock onto to either the plume or the aircraft surface.

Figure 6(a) shows the variation of the ratio of potential plume core IR signature in MWIR band to aircraft surface IR signature in LWIR for $\varepsilon_{acs} = 1$. The radiation ratio (MWIR/LWIR) continuously decreases with M_∞. The trend is similar for both max dry and max reheat mode, and differ only in the magnitude. In max dry mode, the plume MWIR signature is higher than the aircraft bottom surface LWIR signature up to $M_\infty = 1.1$. Above $M_\infty = 1.1$, the surface's LWIR signature surpasses the plume's MWIR signature. This critical Mach number at which the surface LWIR signature surpasses the plume MWIR signature depends on aircraft surface emissivity, engine power and altitude. The IR signature received by the sensor located away from the aircraft is further attenuated by the atmosphere. The atmospheric transmission in the LWIR band is higher compared to the MWIR band, therefore, the net irradiance received by the sensor decides the band to be used for the lock on. The atmospheric transmission between the aircraft at 6km and the sensor on the ground is calculated using LOWTRAN, the τ_{sky} in the MWIR band is 0.56 and τ_{sky} in the LWIR is 0.85.

Figure 6(b) shows the ratio of the irradiation flux (W/m^2-sr) received by the sensor located on the ground (for $\varepsilon_{acs} = 1$). In the max dry mode, the LWIR irradiance of the aircraft surface received by the sensor is higher than the plume MWIR irradiance. However, in the max reheat mode, the plume MWIR irradiance received by the sensor is always higher than the aircraft bottom surface LWIR irradiance. Therefore, from the bottom view, the LWIR band is more suitable for the lock on compared to the MWIR band in the max dry mode. In the max reheat mode, MWIR band is more suitable than the LWIR band. Normally aircraft operates in the max dry mode; max reheat is occasionally used by the aircraft (for faster climb/acceleration or during a manoeuvre). Thus, from the bottom view of the aircraft, the aircraft surface IR signature in the LWIR band becomes more important than the plume's potential core IR signature in the MWIR band. As the sensor approaches the aircraft, the atmospheric transmission
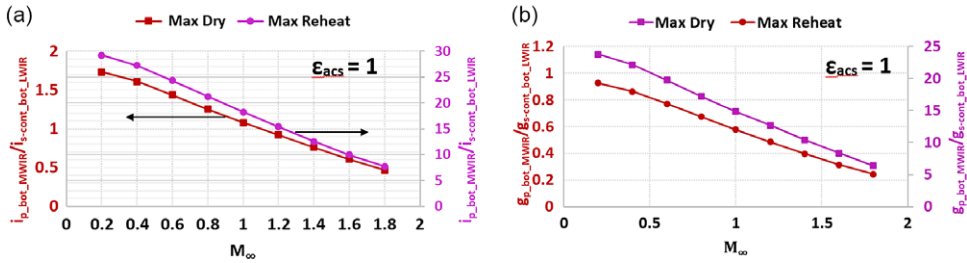
Figure 6. *Variation of ratio of plume (MWIR) to aircraft (LWIR) surface radiation, 6km with M_∞, ISA, $\varepsilon_{acs} = 1$, (a) from the aircraft (b) received by the sensor.*
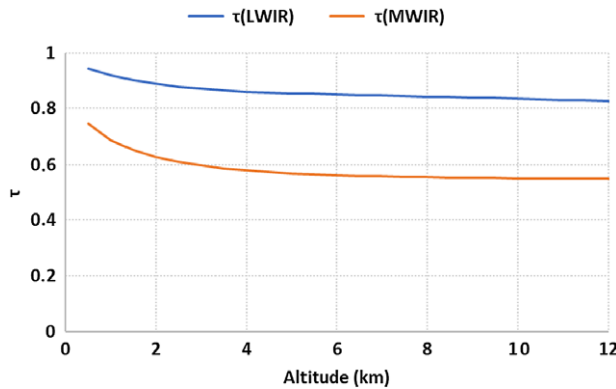

Figure 7. *Variation of atmospheric transmission with altitude.*

increases in both LWIR and MWIR bands (Fig. 7), thus the choice of lock-on between plume and surface may further change. The atmospheric transmission in the LWIR band is higher than the MWIR band.

The plume's potential core IR signature in max reheat mode is significantly higher than the surface radiation; thus, max reheat mode should be avoided when entering or flying over a SAM zone. If the dual-band sensor operates in the SWIR and LWIR bands, the SWIR band is not effective in detecting plume radiation in the max dry mode. However, in max reheat mode, the plume signature becomes significant in the SWIR band as well. Figure 8 shows the variation of the ratio of potential plume core SWIR radiation to aircraft surface LWIR radiation. The plume potential core SWIR band signature is always higher than the aircraft surface LWIR signature for almost all M_∞. At $M_\infty = 1.8$ the radiation ratio (SWIR/LWIR) is less than 1.0. In max reheat mode, both the plume MWIR and SWIR band signatures are higher than the aircraft external surface LWIR signature. Thus, max reheat mode should always be avoided when approaching a SAM site.

The plume MWIR to aircraft external surface LWIR radiation ratio depends on the aircraft surface emissivity. Figure 9 illustrates it for different ε_{acs} (for the max dry mode). It can be observed that for $\varepsilon_{acs} = 1.0$ and 0.5, the plume potential core MWIR signature is higher than the aircraft bottom surface LWIR signature at subsonic M_∞. The radiation ratio (MWIR/LWIR) decreases with increase in M_∞. When $\varepsilon_{acs} \leq 0.2$, the plume radiation is nearly equal to the surface radiation at low M_∞, but becomes higher than the surface radiation as the M_∞ increases. This is because the aircraft surface radiance is a combination of skin emission and earthshine. At low M_∞, the skin emission is very low due to low surface emissivity and lower surface temperatures, but the earthshine reflection is high due to high reflectivity ($\rho_{acs} = 1 - \varepsilon_{acs}$) of the aircraft surface. The earthshine reflection is calculated assuming an earth surface temperature of 30°C, and the aircraft surface self emission is calculated using recovery temperature at 6km altitude. When $\varepsilon_{acs} \leq 0.2$, the ratio (plume MWIR to surface LWIR) increases with increase
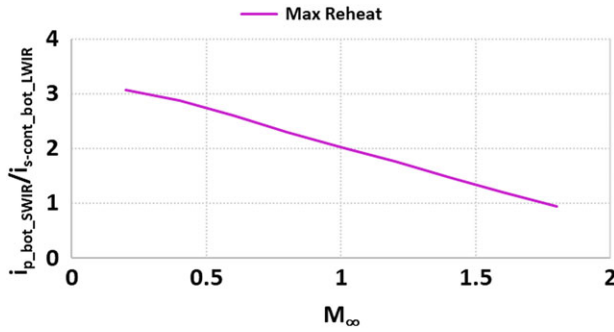
Figure 8. *Variation of ratio of plume (SWIR) to aircraft (LWIR) surface radiation, 6km with M_∞, ISA, $\varepsilon_{acs} = 1$, max reheat.*
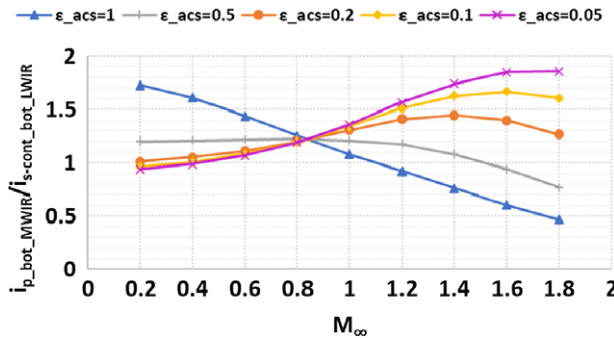

Figure 9. *Variation of ratio of plume (MWIR) to aircraft surface (LWIR) radiation, with M_∞ for different ε_{acs}.*

in the M_∞. It reaches its peak at a specific M_∞ and then decreases. This is because, for $\varepsilon_{acs} \leq 0.2$, as M_∞ increases, the plume emission also increases, and the contribution of the aircraft surface self emission is significantly less compared to the earthshine reflection. The earthshine component is independent of M_∞. As a result, the radiation ratio (MWIR/LWIR) continuously increases until a certain M_∞, at which the skin-emission component starts to contribute, causing the radiation ratio (MWIR/LWIR) to decrease (Fig. 9).

The dual-band sensor can be a combination of any two out of the SWIR, MWIR and the LWIR band. The plume and aircraft hot surface emission is seen in the MWIR and the SWIR band; the only difference is that the plume emission is more prominent in the MWIR band. At high speed, aerodynamically heated surfaces also emit in the MWIR band. Thus, having SWIR-MWIR as a dual-band sensor does not provide any additional advantage for aircraft detection. Combining the LWIR band with the SWIR or MWIR band provides the advantage that the aircraft surface heated due to aerodynamic heating can also be identified in addition to the hot engine components and exhaust plume. The plume SWIR emission is very low in the max dry mode compared to the MWIR emission; the SWIR plume emission is significant only in the max reheat mode. Out of the three combinations of dual IR bands, the MWIR-LWIR combination will be able to detect the plume from the max dry mode to the reheat mode of the engine. If the plume is shielded by the aircraft from the frontal view, the LWIR band will be able to detect the aircraft surfaces from the frontal aspect. Overall, over the wider range of aircraft speed and engine power, the MWIR-LWIR dual band combination is best suited to identify and ascertain the target. The MWIR-LWIR dual band is providing all aspects and all-weather capability to the missile.

The position of the sensor relative to the aircraft, along with its characteristics such as the signal-to-noise ratio (S/N) and the noise equivalent irradiance (NEI), play a significant role in determining the detection range of the aircraft. If other parameters of sensor are constant, smaller the NEI, larger is the detection range of the target. The sensing technology of the MWIR band is completely different than the LWIR band. The MWIR camera detectors use indium antimonide (InSb), lead selenide (PbSb), or mercury cadmium telluride (HgCdTe) to sense thermal emissions. Since the sensing technology of the MWIR and the LWIR sensors is different, their respective noise equivalent irradiance (NEI) values may also be different. Therefore, the lock-on range should be studied on the basis of specific characteristics of each sensor. Also, once the missile/sensor starts chasing the target, the atmospheric attenuation continuously changes the IR signature received by the missile. From the point of view of a hit leading to a kill, it is always beneficial to lock on to the aircraft surface towards the terminal guidance of the missile. If a missile directly hits the aircraft surface, it will cause greater damage to the aircraft. However, if the missile detonates near the plume, the explosion could cause minimal harm since the length of the plume can be equivalent to or greater than that of the aircraft. Since the LWIR band can detect the aircraft surfaces, in a dual-band IR detector or missile, the LWIR band will always provide an advantage for the terminal guidance of the missile.

5.0 Conclusion

- In the MWIR band, the ratio of plume to surface IR radiation decreases as M_∞. increases. At low M_∞., the potential core radiation is higher than the surface radiation. However, for $M_\infty.> 1$, the surface radiation also contributes significantly to the IR signature of the aircraft, eventually becoming comparable to the plume radiation at higher supersonic M_∞.

- In the LWIR band, surface radiation is significantly higher than the plume radiation. Plume potential core is transparent to IR radiation in the LWIR band in max dry as well as max reheat mode.

- When $\varepsilon_{acs} = 1$, in the max dry mode, the plume MWIR emission at low M_∞ is higher than the surface LWIR emission. As the M_∞ increases, the plume MWIR to surface LWIR emission ratio decreases. At supersonic Mach numbers, the surface LWIR radiation is higher than the plume MWIR radiation. When $\varepsilon_{acs} < 0.5$, the plume MWIR emission is higher than the surface LWIR radiation for all M_∞.

- In the max reheat mode ($\varepsilon_{acs} = 0.5$), the plume MWIR as well as SWIR emission is higher than surface LWIR emission for all range of M_∞ under study.

- When the aircraft surface emissivity is unity, the plume MWIR radiation is higher than the surface LWIR radiation for subsonic M_∞. However, sensor located 6km directly below the aircraft receives higher radiation from the surface (in max dry mode). It is because, the atmospheric attenuation is higher in the MWIR band compared to the LWIR band.

- In the max reheat mode, the plume MWIR radiation is significantly higher than the surface LWIR emission. Despite high absorption through the atmosphere, the MWIR emission from the plume received by the sensor positioned 6km directly below the aircraft, exceeds the LWIR radiation.

- The MWIR-LWIR dual band combination is the best suited combination for a dual band IR sensor/detector for aircraft application. It enables sensor to view aircraft as well as the exhaust plume for a range of Mach number and engine power. The combination provides all-aspect all-weather capability to the detector.

References

[1] Rogalski, A. History of infrared detectors, *Opto-Electron. Rev.*, 2012, **20,** (3), pp 279–308.

[2] Mahulikar, S.P. and Sonawane, H.R. Infrared signature studies of aerospace vehicles, *Progr. Aerospace Sci.*, 2007, **43**, (7-8), pp 218–245.

[3] Mahulikar, S.P., Rao, G.A., Sane, S.K. and Marathe, A.G. Aircraft plume infrared signature in non-afterburning mode, *J. Thermo-Phys. Heat Transfer*, 2005, **19**, (3), pp 413–415.

[4] Rao, G.A. and Mahulikar, S.P. Effect of atmospheric transmission and radiance on aircraft infrared signatures, *J. Aircrafts*, 2005, **42**, (4), pp 1046–1054.

[5] Winterfeldt, D., and Sullivan, T.M. Should we protect airplanes against surface to air missile attack by terrorists? *Decision Anal. Informs*, 2006, **3**, (2), pp 63–75.

[6] Cha, J.H., Kim, T., Bae, J.Y., Kim, T. et al., Variation of supersonic aircraft skin temperature under different mach number and structure, *J. Korea Inst. Mil. Sci. Technol.*, 2014, **17**, (4), pp 463–470.

[7] Lu, J. and Wang, Q. Aircraft-skin infrared radiation characteristics modeling and analysis, *Chin. J. Aeronaut.*, 2009, **22**, (5), pp 493–497.

[8] Bhatt, A. and Mahulikar, S.P. Analysis of aero engine plume potential core infrared signature, *Aircraft Eng. Aerospace Technol.*, 2024, **96**, (3), pp 491–498.

[9] Mahulikar, S.P., Rao, G.A. and Kolhe, P.S. Infrared signatures of low flying aircraft and their rear fuselage skin emissivity optimization, *J. Aircraft*, 2006, **43**, (1), pp 226–232.

[10] Kim, T., Lee, H., Bae, J.Y., Kim, T., Cha, J., Jung, D. and Cho, H.H. Susceptibility of combat aircraft modeled as an anisotropic source of infrared radiation, *IEEE Trans. Aerospace Electron. Syst.*, 2016, **52**, (5), pp 2467–2476.

[11] Yanwan, Y. and Yiyun, L. Generation of realistic infrared image for moving objects, *Int. J. Infrared Millimeter Waves*, 2004, **25**, (7), pp 1087–1097.

[12] Kajal, V. and Mahulikar, S.P. Analysis of infrared signature from aircraft frontal aspect due to skin friction heating, *SAE Int. J. Aerospace*, 2023, **16**, (1), pp 3–20.

[13] Li, N., Su, Z., Chen, Z. and Han, D. A real-time aircraft infrared imaging simulation platform, *Optik*, 2013, **124**, pp 2885–2893.

[14] Huang, W. and Ji, H. Impact of background radiation on the long wave infrared radiation characteristics of aircraft at high altitude, *Defence Sci. J.*, 2016, **66**, pp 51–56.

[15] Zhao, Y. and Zheng, S.-J. Nozzle dimension design for aircraft engine infrared signature and thrust active control using MOEA/D, *Proc. Inst. Mech. Eng. Part G–J. Aerospace Eng.*, 2020, **234**, (15), pp 2133–2138.

[16] Wang, H., Ji, H. and Lu, H. Experimental investigation on infrared radiation characteristics of two-dimensional convergent–divergent vectoring nozzle, *J. Thermophys. Heat Transfer*, 2019, **33**, (3), pp 1–11.

[17] Lin, J., Tan, Y.-H. and Tian, J.-W. Coarse to fine aircraft detection from front-looking infrared images, *Infrared Phys. Technol.*, 2018, **89**, pp 181–193.

[18] Cheng, W., Wang, Z.-X., Zhou, L., Sun, X.-L. and Shi, J.-W. Investigation of infrared signature of serpentine nozzle for turbofan, *J. Thermophys. Heat Transfer*, 2019, **33**, (1), pp 170–178.

[19] Haq, F. and Huang, J. Parametric design and IR signature study of exhaust plume from elliptical-shaped exhaust nozzles of a low flying UAV using CFD approach, *Results Eng.*, 2022, **13**, p 100320.

[20] Yue, Z., Qiang, W. and Ting, L. A new model to simulate infrared radiation from an aircraft exhaust system, *Chin. J. Aeronaut.*, 2017, **30**, (2), pp 651–662.

[21] Mahulikar, S.P., Rastogi, P. and Bhatt, A. Aircraft signature studies using infrared cross-section and infrared solid angle, *AIAA J. Aircraft*, 2022, **59**, pp 126–136.

[22] Mahulikar, S.P., Rao, G.A., Sane, S.K. and Marathe, A.G. Aircraft plume infrared signature in non-afterburning mode, *J. Thermo-Phys. Heat Transfer*, 2005, **19**, (3), pp 413–415.

[23] Heragu, S.S., Rao, K.V.L. and Raghunandan, B.N. Generalized model for infrared perception from an engine exhaust, *J. Thermo-Phys. Heat Transfer*, 2002, **16**, (1), pp 68–76.

[24] Decher, R. Infrared emissions from turbofans with high aspect ratio nozzles, *AIAA J. Aircraft*, 1981, **18**, (12), pp 1025–1031.

[25] Johansson, M. and Dalenbring, M., Calculation of IR Signatures from Airborne Vehicles, SPIE paper, 6228-40, 2006.

[26] Rao, G.A. Infrared signature modeling and analysis of aircraft plume, *Int. J. Turbo Jet Engines*, 2011, **28**, pp 187–197.

[27] Mei, F., Chen, S., Jiang, Y. and Cai, J. A preliminary model of infrared image generation for exhaust plume, *Int. J. Image Graphics Signal Process.*, 2011, **4**, pp 46–52.

[28] Avital, G., Cohen, Y., Gamss, L., Kanelbaum, Y., Macales, J., Trieman, B. and Yaniv, S. Experimental and computational study of infrared emission from under-expanded rocket exhaust plumes, *J. Thermo-Phys. Heat Transfer*, 2001, **15**, (4), pp 377–383.

[29] Zhang, J., Qi, H., Jiang, D., Gao, B., He, M., Ren, Y. and Li, K. Integrated infrared radiation characteristics of aircraft skin and the exhaust plume, *Materials*, 2022, **15**, p 7728.

[30] Mahulikar, S.P., Potnuru, S.K. and Rao, G.A. Study of sunshine, skyshine, and earthshine for aircraft infrared detection, *J. Opt.*, 2009, **11**, p 045703.

[31] Mahulikar, S.P., Rastogi, P., Bhatt, A. and Valodhi, S.P. Aircraft visibility in view from below in long-wave infrared band using infrared cross section, *Appl. Opt.*, 2022, **61**, pp 4784–4795.

[32] Kneizys, F.X., Shettle, E.P., Abreu, L.W., Chetwynd, J.H., Anderson, G.P., Gallery, W.O., Selby, J.E.A. and Clough, S.A. User guide to LOWTRAN 7, Hanscom, Massachusetts: Air Force Geophysics Laboratory, 1988.

[33] Berger, X., Bathiebo, J., Kieno, F. and Awanou, C.N. Clear sky radiation as a function of altitude, *Renewable Energy*, 1992, **2**, pp 139–157.

[34] Bhatt, A. and Mahulikar, S.P. Study of statistical narrow-band models for infrared signature of an aeroengine exhaust plume in mid-wave infrared and short-wave infrared band, *SAE Int. J. Aerospace*, 2023, **16**, (1), pp 21–38.

[35] Kurzke, J. and Halliwell, I. *Propulsion and Power an Exploration of Gas Turbine Performance Modeling*, Springer International Publishing, Gasturb14, 2018, Cham, Switzerland.

[36] Philippe, D. and Cathonnet, M. The ignition, oxidation, and combustion of kerosene, a review of experimental and kinetic modeling, *Progr. Energy Combust. Sci.*, 2006, **32**, pp 48–92.

[37] Jackson, H.T. An Analytical Model for Predicting the Radiation from Jet Plumes in the Mid-Infrared Spectral Region, RN-RE-TR-70-07, April 1970.

[38] Taine, J. A line-by-line calculation of low-resolution radiative properties of CO2-CO transparent non-isothermal gases mixtures up to 3000 K, *J. Quant. Spectrosc. Radiat. Transfer*, 1983, **30**, pp 371–379.

[39] Gordon, I. E., Rothman, L. S., Hill, C., Kochanov, R. V., Tan, Y., Bernath, P. F., ... & Zak, E. J. The HITRAN2016 molecular spectroscopic database, *J. Quant. Spectrosc. Radiat. Transfer*, 2017, **203**, pp 3–69.